TWELFTH EUROPEAN ROTORCRAFT FORUM

Paper No. 30

UNSTEADY THREE-DIMENSIONAL STALL ON A RECTANGULAR WING

J.J. Costes

Office National d'Etudes et de Recherches Aérospatiales

BP 72. F - 92322 Châtillon Cedex, France

September 22 - 25, 1986

Garmisch-Partenkirchen
Federal Republic of Germany

Deutsche Gesellschaft für Luft- und Raumfahrt e. V. (DGLR)
Godesberger Allee 70, D-5300 Bonn 2, F.R.G.

DECROCHAGE INSTATIONNAIRE TRI-DIMENSIONNEL SUR UNE AILE RECTANGULAIRE

J.J. Costes
Office National d'Etudes et de Recherches Aérospatiales
BP 72. F - 92322 Châtillon Cedex, France

Résumé

On étudie le décrochage stationnaire et instationnaire dans le cas d'une aile rectangulaire en attaque droite. L'aile peut osciller en tangage autour de l'axe du quart avant. Les expériences ont été réalisées dans la soufflerie S2 de Chalais-Meudon, la vitesse du vent étant de 95 m/s. Elles sont en bon accord avec les résultats fournis par une théorie dont les principes sont exposés dans cet article.

UNSTEADY THREE-DIMENSIONAL STALL ON A RECTANGULAR WING

by J.J. Costes
Office National d'Etudes et de Recherches Aérospatiales
BP 72. F - 92322 Châtillon Cedex, France

Abstract

Steady and unsteady stall are studied on a rectangular wing in normal flow. The wing is allowed to oscillate in pitch around the quarter chord. Experiments performed at the S2 wind-tunnel in Chalais-Meudon with a rectangular wing and a wind velocity of 95 m/s are in good agreement with the results obtained from the theory developed here.

1. Introduction

Unsteady stall is a difficult and poorly understood phenomenon on a rotating helicopter blade. To gain a better understanding of the aerodynamic mechanisms, fundamental studies on a simpler case have been undertaken at the ONERA Department of Structures. A rigid, rectangular and untwisted wing has been selected for these experiments. The wing may be oscillated in pitch around the quarter chord. Five sections on the wing are instrumented with static pressure tubes to record the mean value of the pressure, and with unsteady transducers to record the unsteady part of the pressure. Measurements have been made with this wing in normal flow and the experimental data obtained on these five spanwise locations are compared with the theory presented below.

2. Theory

Profiles for a helicopter blade are generally designed according to 2-D criteria and later, experiments are performed to verify if these criteria have been met. For large amplitude oscillations of the profile, flow separation occurs periodically and one is obliged to rely primarily on experiments to characterize the profile. Nevertheless, the actual helicopter blade is three-dimensional and it is necessary to develop a theory which, taking the 2-D experimental results as input, would allow the computation of the 3-D aerodynamic forces even in the case of stall. Because of the expected difficulties for a rotating helicopter blade, the task has been first undertaken for a rectangular wing.

Classical linear aerodynamics form the basis of the theory presented here, and the usual assumptions for the compressibility of the fluid and the small amplitude of the perturbations are made. Linear aerodynamics in the form of acceleration potential theory [11-14] is used to compute the downwash velocity of the air, and in the case of small amplitude oscillations, the aerodynamic forces on the wing. Only the details useful to understand the extension from linear to non-linear aerodynamics will be developed in the present paper.

1) Two-dimensional steady theory

a) linear case

Let us define the neutral axis of a profile as being the direction of the wind where the lift force is zero, then the angle between the axis of the wind tunnel and the neutral axis of the profile, is by definition, the aerodynamic incidence α of the profile. A lifting point located at the quarter chord position support a doublet of intensity

$q = -\frac{F}{\rho}$. F is the force per unit length and ρ the density of the fluid. The downwash is computed at the three quarter chord, and on this point, a condition of non separation of the fluid from the profile surface makes possible the determination of the lifting force F.

$$F = \frac{1}{2} \rho \, c \, V_\infty^2 \cdot \frac{2\pi\alpha}{\sqrt{1-M^2}} \qquad (1)$$

c is the chord of the profile
V_∞ is the upstream velocity of the fluid in the wind tunnel
M is the Mach number
α is the incidence measured in radians.

A single lifting line is used to allow extension of the theory to the case of stall.

b) Non-linear case

For thin airfoils, small aerodynamic incidences and subcritical speeds, the lift is independent of the profile considered and equation (1) is valid. However, when the incidence is increased, flow separation occurs on the upper surface and each profile is characterized by a steady C_L curve (fig. 1). If the wake and the separated zone above the airfoil (fig. 2) have both a thickness which remains moderate, then everything occurs as if a new profile with a lower incidence is defined. For this new profile and its associated neutral axis the linear computations are valid. In particular, the induced velocity may be calculated in the same way as has been done for linear aerodynamics, and a non-separation condition can be applied to the fictitious neutral axis of the stalled profile. If $\bar{F}$ is the aerodynamic force measured for the profile at the incidence α, an effective incidence α_{eff} may now be defined as follows :

$$\alpha_{eff} = \frac{\bar{F}\sqrt{1 - M^2}}{\pi \rho \, c \, V_\infty^2}$$

Due to stall $\bar{F}$ is less than F and thus α_{eff} is less than α. Separation of the fluid from the profile may be considered as inducing a loss of incidence equal to $(\alpha - \alpha_{eff})$. More conveniently for later computations, a loss of induced velocity Δw may be defined :

$$\Delta w = V_\infty(\alpha - \alpha_{eff}) = \frac{(F - \bar{F})\sqrt{1 - M^2}}{\pi \rho \, c \, V_\infty} \qquad (2)$$

For given Mach and Reynolds numbers, the experimental curves C_L define, at least in an implicit manner, a relation between $\bar{F}$ and F. Thus, the loss of induced velocity Δw may be computed as a function of F or of α.

2) Three-dimensional steady theory

a) linear case. A rectangular wing in normal flow is considered. The wing supports a lifting line located at the quarter chord position (fig. 3). The lifting line is divided into segments of unequal length. On each segment, the lift force is constant. The acceleration potential theory allows the computation of the downwash velocity at the

collocation points. These points are located at the three quarter chord position of the spanwise centerline of each segment. If a_{ij} is the downwash induced at a collocation point P_j by the lifting segment i which supports a force equal to unity, then the non-separation condition at the point P_j gives :

$$V_\infty \theta_j = \sum_{i=1}^{n} a_{ij} F_i \qquad (3)$$

θ_j is the local geometrical incidence of the wing profile at the point P_j spanwise coordinate. This geometrical incidence is the angle between the local wing-profile neutral axis and the direction of the velocity at infinity upstream. F_i is the lift force per unit length on the segment i. Solving the linear system of equations (3) determines the F_i. Following the interpretation of Prandtl for the force F_i, a local aerodynamic incidence may be defined for the wing by the 2-D equation (1) :

$$\alpha_i = \frac{F_i \sqrt{1 - M^2}}{\pi \rho c V_\infty^2}$$

b) Non-linear case. The same process as in the 2-D non-linear case (§ 2.1.b) will be repeated here. If the wake and the separated zone above the wing are of moderate thickness, then a new neutral axis may be defined for the local wing profiles. This determines an effective geometrical incidence θ_{eff} along the wing span. The difference between the actual geometrical incidence and the effective one is a loss due to stall. Define $\bar{F}_i$ as the aerodynamic force per unit length on segment i, then the $\bar{F}_i$ are solutions of the linear system :

$$V_\infty \Theta_{eff\ j} = \sum_{i=1}^{n} a_{ij} \bar{F}_i \qquad (4)$$

This system of equations is not very convenient to handle, it will be rewritten by combining with the system of equations (3) in the following form :

$$\sum_{i=1}^{n} a_{ij} F_i = V_\infty \theta_j + \sum_{i=1}^{n} a_{ij} (F_i - \bar{F}_i) - V_\infty (\theta - \theta_{eff})_j$$

The term $V_\infty(\theta - \theta_{eff})_j$ is the loss of induced velocity due to stall at the point P_j. Now a fundamental hypothesis is introduced : this loss of induced velocity is assumed to be equal to the loss occurring in 2-D for the same level of lift force. Replacing this term by its value given by equation (2), one obtains :

$$\sum_{i=1}^{n} a_{ij} F_i = V_\infty \theta_j + \left\{ \sum_{i=1}^{n} a_{ij} (F_i - \bar{F}_i) - \frac{(F_j - \bar{F}_j) \sqrt{1 - M^2}}{\pi \rho c V_\infty} \right\} \qquad (5)$$

where $\bar{F} = f(F)$ is a non-linear function of F given by the experimental C_L curves.

The non-linear system (5) is the same as system (3) except for the non-linear correction term :

$$w^*_j = \sum_{i=1}^{n} a_{ij}(F_i - \bar{F}_i) - \frac{(F_j - \bar{F}_j)\sqrt{1 - M^2}}{\pi \rho c V_\infty} \qquad (6)$$

System (5) is much more easily solved than system (4) because the non-linearity is placed in a correction term w^*_j, and because the forces F play in it the principal role. If an approximate value of w^*_j is given, by solving a set of linear equations, the F_i may be obtained. Having the F_i, the $\bar{F}$ are given by the C_L curves and thus an updated value of w^*_j may be computed. Furthermore, one may prove that the absolute value of w^*_j remains small, thus zero as a starting value for w^*_j is a reasonable guess. w^*_j is equal to zero in the case of moderate incidences when $F_i = \bar{F}_i$. In the case of large geometrical incidences along the wing span, separation does occur on the upper surface, but at the wing tip, the aerodynamic lift forces decrease rapidly toward zero and the aerodynamic incidences which are proportional to F are small. According to our very simplified assumptions, no stall can occur at the tip and the corrective factor w^* is thus equal to zero. Let us now consider what happens in the middle of the wing. If we restrict ourselves to the case of a large aspect ratio wing, then the middle of it behaves more or less as a 2-D profile, and the downwash there may be approximated by its 2-D value :

$$\sum_{i=1}^{n} a_{ij} X_i \simeq \frac{X_j \sqrt{1 - M^2}}{\pi \rho c V_\infty}$$

The subscript j stands for the segment of doublets in the middle of the wing. Both terms in equation (6) thus cancel out.

Being small in the middle of the wing as well as at the tips, it is expected that w^* will remain small everywhere. A step by step process may be devised from these considerations in a straightforward way. The value 0 is given to w^*_j at the initial step and at each following step and updated value is computed.

In most cases, the iterative process converges rapidly. Nevertheless, because (5) is a non-linear system, one cannot be sure of the existence and even of the uniqueness of the solution. This is the reason why, only an approximate solution which minimises an error function of system 5 is searched for, instead of an exact one. The error function may conveniently be taken as the sum :

$$\sum_j \{ \sum_{i=1}^{n} a_{ij} F_i - V_\infty \theta_j - w^*_j \}^2$$

Because of the possible multiplicity of local minima, the solution closest to the starting linear solution of system (5) ($w^* = 0$) is retained.

3) Two-dimensional unsteady theory

a) Linear case. A profile is oscillating in pitch around the quarter chord position at a low enough reduced frequency. This allows theoretical computations to be done with a reasonable accuracy by replacing the blade with a single lifting point located at the quarter chord position. The downwash velocity induced by the lifting point is calculated for a collocation point at the three-quarter chord position as in the steady case. Let us suppose the complex number $w(\omega)$ be the velocity induced by a doublet of intensity $-\frac{e^{j\omega t}}{\rho}$.

A non-separation condition makes possible the calculation of the unsteady lift.

$$\left(V_\infty + j\,\omega\,\frac{c}{2}\right)\alpha_o\, e^{j\omega t} = \mathcal{W}(\omega)\, F(t) \qquad (7)$$

where $\alpha(t) = \alpha_o\, e^{j\omega t}$ is the incidence of the profile, and $F(t) = F_o\, e^{j\omega t}$ is the unsteady lift (F_o is a complex number). This allows the determination of the complex number $C_L(\omega)$, the 2-D unsteady lift coefficient for a thin airfoil. Due to the single lifting line hypothesis, the method of computation presented here does not give accurate results for values of the reduced frequency $\frac{\omega c}{2 V_\infty} > 0.3$.

b) Non-linear case

Now, the variations of the incidence $\alpha(t)$ are large enough to induce a periodical separation of the flow from the profile upper surface. The value of the lift as a function of the time t is assumed to be given by an experiment performed in a wind-tunnel. Such experiments have generally been performed only for a limited number of cases. The parameters of the experiment are the amplitude and the frequency of the harmonic oscillations, the mean value of the incidence, and the Mach and Reynolds numbers. The difficulties linked to the use of numerical tables, and the need for parameters which are not in the set of experimental data, makes necesary the use of a model able to give the lift (and the moment), for any kind of periodical, but not necessarily harmonic movement of the airfoil. Such a model has been developed at the ONERA Department of Structure by D. Pétot et al. [4-7]. The lift and the moment for the profiles are represented by using coupled non-linear differential equations. Only a limited number of experimental results including the steady lift and moment curves and some oscillations of small (or even large) amplitude around a given mean incidence are necessary to determine the coefficients of the differential equations. This model is used in the work presented here.

Now, let us suppose that for an incidence $\alpha(t)$ a lift force $\bar{F}(t)$ is obtained. Generally, the non-linear lift has a modulus smaller than the linear one : $|\bar{F}(t)| < F(t)$.

As in the steady case, it is supposed that the thickness of the separated zone and that of the wake remain moderate, then an effective incidence may be defined for the profile. The problem is now the following one : taking the time-history of $\bar{F}(t)$ as given, determine the effective incidence $\alpha_{eff}(t)$ time-history. By definition, the effective incidence is the incidence which would create the observed lift force when the linear equation (7) between incidences and forces is used. The computation of the effective incidence will be done in the following way :

Only periodic functions of time with a limited number of harmonic components are considered. If m is the number of harmonics and T the period of the function, a set of time steps τ_i is introduced :

$$\tau_i = \frac{(i-1)\,T}{2m+1}$$

The time steps τ_i are used in the definition of a set of periodical functions of time $g_i(\tau)$ with only m harmonic components which satisfy the conditions :

$g_i(\tau)$: 1 if $\tau = \tau_i$

$g_i(\tau) = 0$ if $\tau = \tau_j$; $i \neq j$.

As an example, one of these functions is represented in fig. 4, the other functions with the same number or harmonics may be deduced by

translation.

The experimental lift force $\bar{F}(\tau)$ may be decomposed on the basis of the functions $g_i(\tau)$, which is equivalent to neglecting the harmonics of rank m + 1 and higher.

$$\bar{F}(\tau) = \sum_{i=1}^{2m+1} \bar{F}(\tau_i)\, g_i(\tau) \tag{8}$$

The downwash velocity, induced on the three quarter chord collocation point by a doublet of intensity $-\frac{g_i(\tau)}{\rho}$, may be obtained by addition of the velocities induced by each harmonic component of $g_i(\tau)$. Let $\mathcal{W}_i$ be this velocity, a linear non-separation condition may be written for the effective incidence at some instant t :

$$V_\infty\, \alpha_{eff}(t) + \frac{c}{2}\, \frac{d}{dt}\, \alpha_{eff}(t) = \sum_{i=1}^{2m+1} \bar{F}(\tau_i)\, \mathcal{W}_i(t) \tag{9}$$

The incidence $\alpha_{eff}(t)$ can be decomposed on the basis of functions $g_i(t)$. Then, if equation (9) is written for 2m+1 instants t, one obtains a set of simultaneous linear equations whose solution determines the function $\alpha_{eff}(t)$. In fact it is not necessary to pursue the computations up to the complete determination of $\alpha_{eff}(t)$. What will be needed for the 3-D extension of the theory is the loss of induced velocity. In the linear case the induced velocity is given by :

$$V_\infty\, \alpha\,(t) + \frac{c}{2}\, \frac{d}{dt}\, \alpha(t) = \sum_{i=1}^{2m+1} F(\tau_i)\, \mathcal{W}_i(t) \tag{10}$$

The loss of induced velocity is given by the difference between equations (10) and (9) and may be written as :

$$\Delta\mathcal{W}(t) = V_\infty[\alpha(t) - \alpha_{eff}(t)] + \frac{c}{2}\, \frac{d}{dt}[\, \alpha(t) - \alpha_{eff}(t)] = \tag{11}$$

$$\sum_{i=1}^{2m+1} [\, F(\tau_i) - \bar{F}(\tau_i)]\, \mathcal{W}_i(t)$$

The linear force F(t) is related to the incidence of the profile by the relation (10). The incidence of the profile determines also the experimental force $\bar{F}(t)$, then $\bar{F}(t)$ may be considered as a function of F(t) and through equation (11), $\Delta\mathcal{W}(t)$ is also a function of F(t).

4) Three-dimensional unsteady theory

The wind velocity at infinity is constant and the wing has an oscillatory motion in pitch around the quarter chord line. The theory will be presented first in the linear case, and then will be extended to take into account the effects of stall.

a) Linear case. As in steady flow, the wing is replaced by a single lifting line located at the quarter chord position. The lifting line is divided into segments of unequal length. On each segment, the lift is constant along the spanwise direction, but it varies periodically with time. Only a limited number of harmonics is considered, and thus the functions $g_i(\tau)$ presented in the preceding paragraph may be used. If $F_j(\tau_i)$ is the value of the lift force per unit length on the segment j at the instant τ_i, then at any instant τ the lift on the segment j is given by :

$$F_j(\tau) = \sum_{i=1}^{2m+1} F_{ji}\, g_i(\tau) \tag{12}$$

At a time t, the downwash velocity $w_{ij}(t, y)$ induced at a collocation point P by a lift force equal to $g_i(\tau)$ on the segment j and equal to zero on the remaining of the lifting line may be computed. As in steady flow, the collocation points are located on the three-quarter chord position of the spanwise centerline of each segment. If $\theta(t, y)$ is the geometrical incidence of the local wing profile, a non-separation condition may be written :

$$V_\infty\, \theta(t, y) + \frac{c}{2}\, \frac{\partial}{\partial t}\, \theta(t, y) = \sum_{i=1}^{2m+1} \sum_{j=1}^{n} F_{ji}\, w_{ij}(t, y) = w(t, y) \tag{13}$$

As in 2-D, the non-separation condition includes unsteady terms dependent on the derivative of the incidence.

b) Non-linear case. In the case of stall, the lift on a segment j is given in a form equivalent to equation (12) by :

$$\bar{F}_j(\tau) = \sum_{i=1}^{2m+1} \bar{F}_{ji}\, g_i(\tau)$$

An assumption of moderate thickness, for the wake and the separated zone on the wing upper surface, allows the computation of the downwash velocity $\bar{w}(t, y)$ as in linear conditions :

$$\bar{w}(t, y) = \sum_{i=1}^{2m+1} \sum_{j=1}^{n} \bar{F}_{ji}\, w_{ij}(t, y) \tag{14}$$

Here, contrary to what was true in the linear case, equation (13), the total downwash velocity can no longer be given by a non-separation condition. Instead of the actual geometrical incidence of the wing, an effective incidence should be considered. The difference between the actual and the effective incidence is a loss due to stall. A way to express this analysis in a mathematical form is to say that to the velocity $\bar{w}(t, y)$ a loss of induced velocity must be added, the sum of both terms being equal to the usual non-separation condition. As in the steady case, a fundamental assumption is now made : the loss of induced velocity in 3-D is assumed to be the same as in 2-D for the same profile at the same aerodynamic incidence $\alpha(t)$. The loss of induced velocity is given by (11) and one may now write the following non-linear equation :

$$V_\infty\, \theta(t, y) + \frac{c}{2}\, \frac{\partial}{\partial t}\, \theta(t, y) = \sum_{i=1}^{2m+1} \sum_{j=1}^{n} \bar{F}_{ij}\, w_{ij}(t, y) + \sum_{i=1}^{2m+1} (F_{ji} - \bar{F}_{ji})\, \mathcal{W}_i(t) \tag{15}$$

where F_{ji} and $\bar{F}_{ji}$ are the linear and non-linear lift forces on the segment j at the time τ_i. $\bar{F}_{ji}$ is a function of the time history of the local profile incidence, that is to say of the linear lift forces F_{ji} ; i = 1, 2m + 1.

$$\bar{F}_{ji} = f_j(F_{j1} \; ; \; 1 = 1, \ldots\ldots, \; 2m + 1, \; \tau_i) \tag{16}$$

When the profile is the same along the wing span, and this is the case for our experimental model, the function f does not depend on the spanwise location and the subscript j may be omitted in f_j.

Let us suppose that the time history of the aerodynamic incidence $\alpha(t)$ is known. Then the linear lift force $F(t)$ may be computed and the non-linear lift $\bar{F}(t)$ may also be obtained from $\alpha(t)$ by means of the mathematical model developed at ONERA. In the present computation, the linear lift force $F(t)$ is given instead of $\alpha(t)$, and the linear equation (10) allows the determination of $\alpha(t)$ when the number of harmonics is limited. The functions $g_i(\tau)$, used in the non-linear 2-D case are are also used here. Through this indirect process, the determination of $\bar{F}(t)$ as a function of $F(t)$ is possible. On the contrary, the reverse process, the determination of $F(t)$ as a function of $\bar{F}(t)$ is generally not feasible. Equation (15), where the $\bar{F}$ are playing the most important role is thus not convenient for the numerical computations, it will be transformed into equation (17) by combination with the linear equation (13) :

$$\sum_{i=1}^{2m+1} \sum_{j=1}^{n} F_{ji}\, w_{ij}(t, y) = V_\infty\, \theta(t, y) + \frac{c}{2} \frac{\partial \theta}{\partial t}(t,y) \qquad (17)$$

$$+ \sum_{i=1}^{2m+1} \sum_{j=1}^{n} (F_{ji} - \bar{F}_{ji})\, w_{ij}(t, y) - \sum_{i=1}^{2m+1} (F_{ji} - \bar{F}_{ji})\, \mathcal{W}_i(t)$$

Let :

$$\mathcal{W}^*(t, y) = \sum_{i=1}^{2m+1} \sum_{j=1}^{n} (F_{ji} - \bar{F}_{ji})\, w_{ij}(t, y) - \qquad (18)$$

$$- \sum_{i=1}^{2m+1} (F_{ji} - \bar{F}_{ji})\, \mathcal{W}_i(t)$$

In equation (17), the term $\mathcal{W}^*$ may be considered as a correction factor which may be determined as soon as approximate values for the F_{ji} and $\bar{F}_{ji}$ are known. Then, the solution of equation (17) gives an updated value of the F_{ji}, and by means of the ONERA stall model, of the $\bar{F}_{ji}$. The cycle is repeated until convergence. Equation (17) must be written for the n collocation points and for the $2m + 1$ instants τ_i. This iterative process has already been used in the steady case, but does not generally gives satisfactory results here. The reason is that $\mathcal{W}^*$ may become very important when the oscillations of the wing are of large amplitude. This compromises the stability of the method. To overcome these difficulties, a generalized Newton method has been used and is presented below.

Let the F_{ji} be an approximate solution of the system of equations (17). The non-linear forces $\bar{F}_{ji}$ are deduced from the F_{ji}, and an error for each of the system equations is computed. Now, a new solution is sought in the form $(F_{ji} + \delta F_{ji})$ which yields $(\bar{F}_{ji} + \delta \bar{F}_{ji})$ for the non-linear forces with :

$$\delta \bar{F}_{ji} = \sum_{i=1}^{2m+1} \frac{\partial f}{\partial \bar{F}_{ji}} (F_{j1} \cdots F_{j\,2m+1}, \tau_i)\, \delta F_{ji} \qquad (19)$$

The evaluation of equation (19) must be done by a process independent from the method of modelization chosen for the experimental 2-D lift forces. This is why the partial derivatives in equation (19) will be calculated by finite differences. Using this method, the non-linear system of equations (17) is transformed into a linear one where the variables δF_{ji} are to be determined. In the following calculation step, the process is repeated starting from the new approximate solution $(F_{ji} + \lambda \delta F_{ij})$, where λ is a relaxation parameter whose value is less than or equal to 1.

As as been mentioned, at each step, the absolute value of the error is evaluated and calculation is continued up to the closest local minimum (calculation begins from the linear solution $W^{*} = 0$). As the existence and uniqueness of the solution of the system of equations (17) cannot be assured, the method used here has the merit of supplying a possible approximate solution.

2. Experiment - Comparison with the theory

1) Presentation of the model

A rigid, untwisted rectangular wing has been constructed for the investigation of the stall phenomena and for testing the theory. The profile is an OA 209 along the complete wing span. Oscillations in pitch around a line located at the quarter chord can be imposed by means of a hydraulic actuator. The amplitude of the movement is limited to $\pm$ 5° around a mean incidence. The absolute value of the incidence is in every case less than 23°. Five sections (fig. 5) are instrumented with 33 static pressure tubes which give the average value of the pressure, and with 23 unsteady pressure transducers to record the unsteady part of the pressure. The pressure distribution along the upper and lower surfaces of the instrumented sections is available, but only the integrated results (lift and moment), can be compared with the results furnished by the simplified theory presented in the preceding chapter. During the experiments, any bending of the wing was prevented by three guy wires. Moreover, accelerometers located inside the wing were able to detect the torsional deformations, at least when the frequency of the wing pitch oscillations was high enough for good sensitivity of the accelerometers. Though some deformations were detected, they are considered small enough to be neglected.

2) Steady stall

A preliminary experiment was performed in November 1983 and more complete results were obtained in February and March 1985. Both experiments took place in the S2 wind-tunnel at Chalais-Meudon. The wind speed was 95 m/s and the Mach number 0.3. Although some problems were expected when the incidence of the wing was large enough to induce a separation of the flow on the upper surface, the extent of the scatter of the results for incidences greater than 15° came as a surprise. In an effort to reduce this scatter the transition of the boundary layer from a laminar to a turbulent flow was forced by a strip of carborundum powder located close to the leading edge (5% chord). Indeed, this significantly reduced the scatter in the data, but a close examination of the pressure distribution on the upper surface showed that the flow was separating from the wing upper surface at the trip strip. This was clearly artificial and too far from the actual conditions on a helicopter blade. For the second experiment in 1985, another approach was selected, this time the wing surface was maintained as clean as possible, and small amplitude pitch oscillations around a mean given incidence were imposed on the wing. This was in the hope of reducing the extent of the scatter for the lift force and the moments. The oscillations could play a role similar to the grit but are more representative of actual flight conditions on a helicopter blade. Furthermore, some experiments performed at the CEAT in Toulouse [9, 10] with an amplitude of $\pm$ 1° have shown a correlation between the frequency of the oscillation and the mean value of the lift. It was necessary to verify that the lift and moment mean values are, for vanishingly small amplitudes of oscillation, independent of the

frequency. Data were obtained for amplitude of $\pm$ 1° ; $\pm$ 0.5° ; $\pm$ 0.25°. They have proved that indeed the results are independent of the frequency, at least for the low frequency range investigated (f < 50 Hertz ; Reduced frequency $k = \frac{\omega c}{2 V_\infty} < 0.4$), when the amplitude is equal or smaller than 0.5°.

Stall is not really a steady phenomenon and much fluctuation can be seen in the pressure distribution. In an effort to minimize the effects of these fluctuations, a large number of acquisitions (2000 or 4000) were made and averaged. In spite of these large averages, the results obtained for the lift (fig. 6) and for the moments (fig. 7) present a very significant degree of scatter when the incidence is greater than 15°. It is now believed that this phenomenon is characteristic of the steady stall, and that no improvement can be expected by refining the experimental process. It also seems that the small amplitude oscillations applied to the wing during the experiments are not necessary, and they will be omitted in the future. On the contrary, the way by which the prescribed incidence is obtained seems to be very important. Increasing incidences tend to give higher values for the lift and decreasing incidences lower values. It would be interesting to perform an experiment starting from 0° and steadily increasing the incidence up to large angles (23°) and then reversing the operation from 23° to 0°. Both results should be compared to the results obtained by chosing the incidence at random. In the 1985 experiment, the incidences were obtained in a more or less random order. As can be seen on figs. 6 and 7, an upper limit and a lower limit can be defined by a smooth curve for the lift and the moment. It may be said for the upper limit that for some unknown physical reason the profile has "forgotten" to stall, and on the contrary for the lower limit the most complete stall has occurred on the profile. The possibility to define a lower limit for the C_L and C_M curves is of considerable interest for the helicopter rotor. The experiments performed with pitch oscillations of large amplitudes have shown, that in each case, the experimental C_L and C_M loops ar roughly centered on the steady C_L and C_M lower limit curves. This may be explained by the following physical reason : in the case of large amplitude oscillations, stall is obliged to fully develop on the upper surface, and thus the C_L and C_M steady values to be taken into account are also those relative to a completely stalled profile. Later in this paper, the steady lift and moment curves will implicitly make reference to the lower limit of the C_L and C_M for the large incidence angles.

Theoretical results obtained by C. Costes are compared to the 1985 experimental data in figs. 6 and 7 and to the 1983 experiment in [2]. Initially the necessary input data, that is to say the 2-D experimental curve for the OA 209 profile was obtained from experiments performed at the CEAT in Toulouse (fig. 8), at a a Reynolds number $R = 2.76\ 10^6$. For the S2 Chalais-Meudon experiment, the Reynolds number is $1.72\ 10^6$ and this may explain the poor agreement obtained between the theory and the experiment. Let us consider the instrumented section 5 ; due to the wind-tunnel wall effect, the effective length of the experimental model is multiplied by 2 and the wing aspect ratio is then equal to 10. In a first approximation, the instrumented section 5 may be considered as a 2-D profile. Important differences may be seen on fig. 8 between the C_L of the CEAT OA 209 2-D profile and the section 5 C_L. This may tentatively be explained by the difference in Reynolds number of the experiments. Because no other 2-D data was available for the OA 209 at the correct Reynolds number, the results of section 5, with some corrections to take into account for the location of this section on a

finite span wing, have been used as input data in the theory. The correction is very simple, if θ is the geometrical incidence of the untwisted wing and α the aerodynamic incidence of section 5, one can write : $\alpha = \theta + \Delta\theta$.

In the case of linear aerodynamics, the correction $\Delta\theta$ is easily computed and has been found to be :

$$\Delta\theta \simeq - 1.49\ C_L \quad \text{(all angles } \alpha, \theta, \Delta\theta \text{ in degrees)} \qquad (20)$$

Equation (20) is valid as long as the lift remains proportional to the wing geometrical incidence all along the wing span. This is true for small angles of incidence ; in the presence of stall, the same correction has also been applied. This would be good if stall could be considered as a phenomenon proportional to the lift which is not the case. However, in the case of very large angles of incidence, the lift remains at a low value approximately independent of the incidence and therefore errors in $\Delta\theta$ will have no effect. Fig. 8 shows the corrected lift curve deduced from the section 5 lift curve by application of equation (20). This curve has been used in the computations presented in this paper as the C_L for the OA 209 profile. The same correction, equation (20), has been applied for the moment coefficient curve (fig. 9). The agreement between the theory and the experiment in fig. 6 is excellent, even for section 1 where the loading is strongly affected by tip vortex effects [3]. As was explained in chapter 2, the local aerodynamic incidence is computed along the wing span, then by means of the C_L and C_M 2-D curves, the local lift and moment are obtained. The moments are given in fig. 7 which also shows good agreement between the theory and the experiment for the inboard sections 5, 4 and 3. Results on section 2 are less satisfactory, and large discrepancies occur for section 1 when the geometrical incidence of the wing is larger than 6°. At the wing tip, due to 3-D effects, the lift and thus the aerodynamic incidence is small. In the very simplified theory presented in this paper, the tip vortex effect is not taken into account. Although no stall is apparent on section 1, the pressure distribution along the chord is strongly affected and this causes large pitching moments even though the lift distribution appears unstalled. Tip vortex effects are probably the explanation of the good correlation in C_L and of the observed discrepancies in C_M at the outboard sections.

3) Unsteady stall

a) Experiment. On a helicopter blade, the aerodynamic incidence on a blade section at a fixed radial location may undergo very large amplitude variations, but at a low frequency. For the wing model a frequency of 4.69 Hertz (reduced frequency 0.039) was chosen. The amplitude of the oscillations was limited to $\pm$ 5°. The mean incidence was varied from 0° up to 18°. A few experiments were also performed for different frequencies and for non sinusoïdal pitch oscillations. In the present paper, only two cases will be presented, both with purely sinusoïdal pitch oscillation. In the first case, the mean value of the wing geometrical incidence is 14°, stall and flow reattachment occur periodically on the wing upper surface. The second case, with a mean incidence of 18°, is easier to deal with, the wing remains in the stalled regime throughout the whole oscillation cycle. The experimental data reduction process used is explained below :

The pressure given by the unsteady transducers is multiplied by the appropriate coefficient and summed to give the unsteady parts of the lift and of the moment. These two values are recorded during a time interval corresponding to about three periods of the oscillation. One example of the results is given in fig. 10. As may be seen on this

figure, unsteady stall is not a repeatable phenomenon, at least for the part of the cycle with decreasing incidences ; this is when flow reattachment occurs. In these experiments, we are more concerned with the averaged values of the lift and moment than with the statistical properties of the scatter. Thus a large number of three period long records (usually 40) are averaged to obtain the definitive lift and moments loops. The final result covers a time interval equal to three cycles of oscillation. If the number of records in the averaging is sufficient, then the three cycles are identical, and represented on the same picture they must superpose on each other. This provides an automatic checking of the experimental data reduction.

b) Comparison with the theory

As for steady stall, one of the most important problems is the choice of the parameters in the 2-D ONERA mathematical model. These parameters are of two kinds, first a steady lift or C_M curve is needed, and then purely unsteady parameters must be defined. The steady lift and moment curves have already been presented in figs. 8 and 9. For the lift, two sets of unsteady parameters have been selected. The first set is the one used in the standard stall model, it is based on experiments performed at the CEAT in Toulouse with a Reynold number R = 2.76 10 ; higher than the Reynolds number R = 1.72 10 for the wing. The second set of parameters have been used in an effort to explain the differences observed between the theory and the results given by the standard parameters on the most inboard instrumented section (section 5). For the moments, only the unsteady parameters of the standard model have been used. In figure 11 are presented the results obtained for the lift, when the incidence of the wing is 14° $\pm$ 5° with a periodic separation and reattachment of the flow. Computations have been done with the standard set of parameters. Both the theory and the experiment show the expected behaviour, that is to say large open loops for the inboard sections 3, 4 and 5, corresponding to the comparatively large aerodynamic incidences On sections 1 and 2, closer to the tip, the aerodynamic incidence is lessened by the three-dimensional effects and the local profile does not penetrate so far into the stall regime. For that reason, the opening of the loops is diminished. For all the sections, the abscissa corresponds to the geometrical incidence of the untwisted wing. As can be seen on figure 11, some important differences appear between the theory and the experiment for the inboard sections. At these locations, the 3-D efects should not be very important, this is why a problem with the unsteady parameters of the 2-D stall model is suspected. In an effort to check the sensitivity of the results to the input parameters, a new set of coefficients has been selected ; they introduce a delay in the onset of stall, and less "damping" in the differential equations which results in a quicker reattachment. The new calculation is presented in figure 12 which shows some improvement when compared with figure 11. For the moments, the results are given in figure 13. A good correlation was not expected but still the theory gives very satisfactory results for the sections 3, 4 and 5. On section 1, the important difference may be explained, as in the steady case, by the effects of the tip vortex. Section 2 is also probably influenced by the large pitching moments at the wing tip. Another case is presented in figures 14 and 15 for a geometrical incidence of the wing equal to 18° $\pm$ 5°. This time, the incidence remains large throughout all the cycle of oscillation and the wing always remains in the stall regime. It is also known, that for large incidences, all the profiles behave approximately in the same way and the unsteady coefficients of the stall model are less dependent on the profile and even on the Reynolds

number. Agreement for the lift (fig. 14) is now particularly good even at the tip. For the moments, the results are also very satisfactory except for section 1, due to the tip vortex effect.

4. Conclusion

The prediction of the aerodynamic forces in the case of 3-D steady and unsteady stall can be achieved by the highly simplified theory presented in this paper. As a starting point, the theory used the experimental results obtained on 2-D profiles. The experimental results are put into a useful form by means of the ONERA mathematical model. The concept of loss of induced velocity allows the extension of the 2-D results to the more difficult case of 3-D stall.

The comparison between the theory and the experiment is satisfactory, but one of the most important aspects of this study has been the emphasis on some of the pertinent experimental details. At large incidences, in the steady case, an important scatter of the experimental results must be expected. This scatter is not an experimental error, but insteady seems to be a fundamental aspect of the stall phenomenon. The value of the lift forces and of the moments depends on the way in which the wing geometrical incidence has been established, that is to say, by increasing or decreasing incidence. The pressure distribution may also depend on the wind-tunnel turbulence, the cleanliness of the wing, and other unknown and possibly random factors. Nevertheless, it seems that for the aerodynamic forces and for the moments, an upper and a lower limit can be defined by smooth curves. For the unsteady stall, and for the important variation of the incidence which appears in the case of the helicopter rotor, only the lowest limit, corresponding to a fully developed stall need be considered. Another noteworthy fact is the necessity for reliable 2-D data, particularly the effect of a variation in Reynolds number should be clarified. This will be done in a new experiment planed to take place in the the Modane S2 wind-tunnel. The next step in this study of 3-D stall is the investigation of the swept flow effects. Some initial experiments have already been performed, and they will be completed in Modane.

References

1. Costes J.J. - Equilibre aéroélastique d'un rotor d'hélicoptère en présence de forces aérodynamique non-linéaires. La Recherche Aérospatiale 1982-5, French and English editions.
2. Costes C., Costes J.J., Pétot D. - Unsteady stall modeling in three-dimensional flow. La Recherche Aérospatiale 1985-4, French and English editions.
3. Adler J.N. and Luttges M.W. - Three-dimensionality in unsteady flow about a wing. AIAA paper 85-0132, 23rd Aerospace Science Meeting, January 14-15, 1985, Reno, Nevada.
4. Dat R., Tran C.T. et Pétot D. - Modèle phénoménologique de décrochage dynamique sur profil de pale d'hélicoptère. XIVe Col. d'Aérodynamique Appliquée, (AAAF), Lille, TP ONERA 1979-149.
5. Tran C.T. and Pétot D. - Semi-empirical model for the dynamic stall of airfoils in view of the application to the calculation of responses of a helicopter in forward flight. 6th European Rotorcraft and Powered Lift Aircraft Forum, Bristol, TP ONERA 1980-103.

6. Pétot D. - Progress in the semi-empirical prediction of the aerodynamic forces due to large amplitude oscillations of an airfoil in attached or separated flow. 9th European Rotorcraft Forum, Stresa, TP ONERA 1983-11.
7. Pétot D. - Modélisation du décrochage dynamque du profil NACA 0012. La Recherche Aérospatiale 1984-6, French and English editions.
8. Gormont R.E. - A mathematical model of unsteady aerodynamics and radial flow for application to helicopter rotors. USA-AMRDL-TR-72-67, May 1973.
9. Coulomb J. - Moyen d'essais pour l'étude de l'écoulement instationnaire autour de profils en oscillations harmoniques. XVIe Col. d'Aérodynamique Appliquée (AAAF), Toulouse 1977.
10. Coulomb J. - Profil 0A 209 essais instationnaires en oscillations harmoniques $\alpha = \pm 1°$. CEAT PV 104/SC.
11. Dat R. - Représentation d'une ligne portante animée d'un mouvement vibratoire par une ligne de doublets d'accélération. La Recherche Aérospatiale, N° 133, 1969. Traduction NASA-TT-F12952, 1970.
12. Dat R. - La théorie de la surface portante appliquée à l'aile fixe et à l'hélice. La Recherche Aérospatilale n° 1973-4. Traduction ESRO-TT-90, 1974.
13. Costes J.J. - Calcul des forces aérodynamiques instationnaires sur les pales d'un rotor d'hélicoptère. AGARD report, n° 595, 1972. Traduction NASA-TT-F-15039, 1973.
14. Costes J.J. - Introduction du décollement instationnaire dans la théorie du potentiel d'accélération. Application à l'hélicoptère. La Recherche Aérospatiale, n° 1975-3.

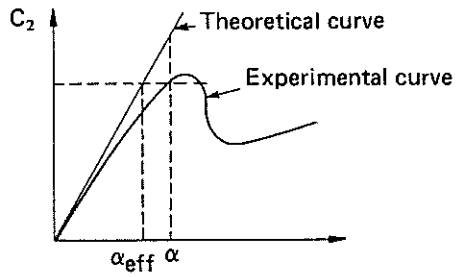

Fig. 1 – Theoretical and experimental lift coefficients. α is the actual aerodynamic incidence ; α_{eff} is the effective aerodynamic incidence of a theoretical airfoil that gives the same C_L as measured on the actual airfoil.

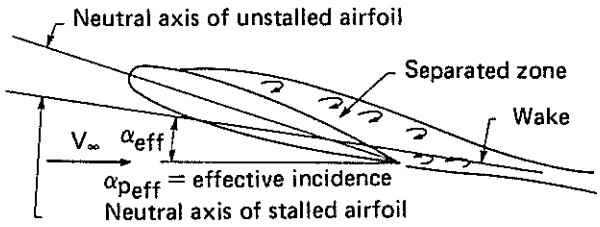

Fig. 2 – Separated flow around a two-dimensional airfoil.

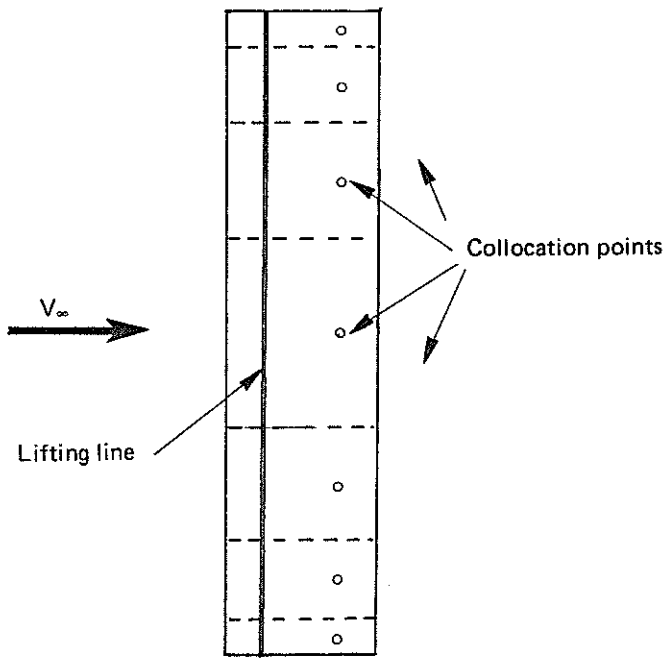

Fig. 3 – The wing is represented by a single lifting line at the quarter chord position. In the spanwise direction, the lift varies in a stepwise fashion. The downwash velocities are calculated at collocation points located on the three-quarter chord line. For clarity, the chord dimension is exaggerated. The correct aspect ratio of the actual wing is shown in Fig. 5.

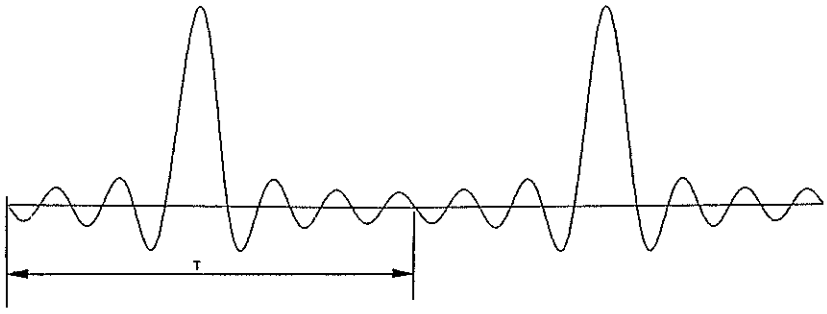

Fig. 4 – Example of function $g(\tau)$. Function $g_\eta(\tau)$ represented here is equal to 1 for $\tau = \tau_\eta + nT$ and to zero for $\tau = \tau_i + nT, i \neq 7$. The function $g_\eta(\tau)$ includes only 6 harmonics.

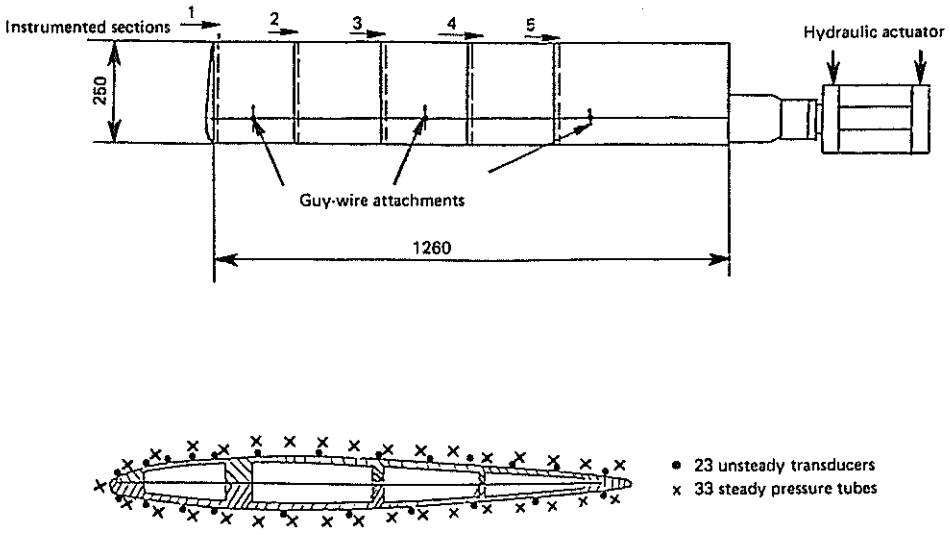

OA 209 profile. Instrumented section

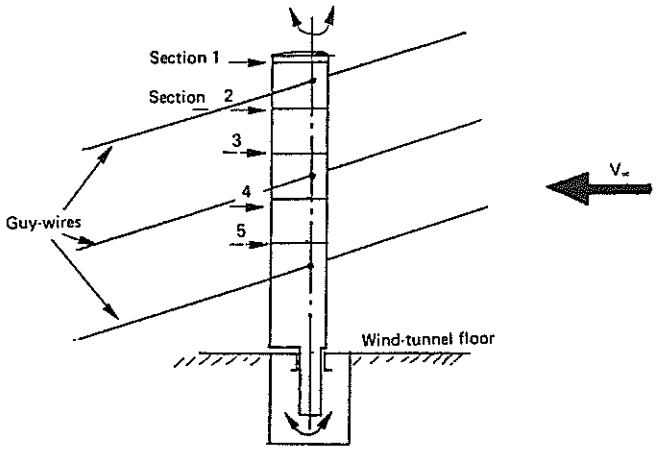

Fig. 5 – This figure shows the experimental model which has been used in unsteady stall studies.

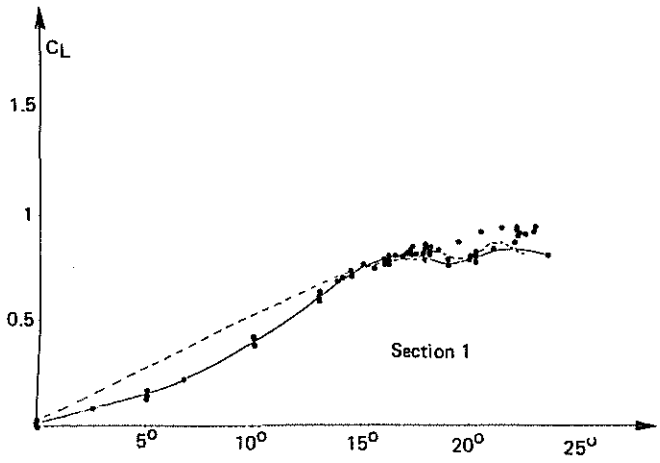

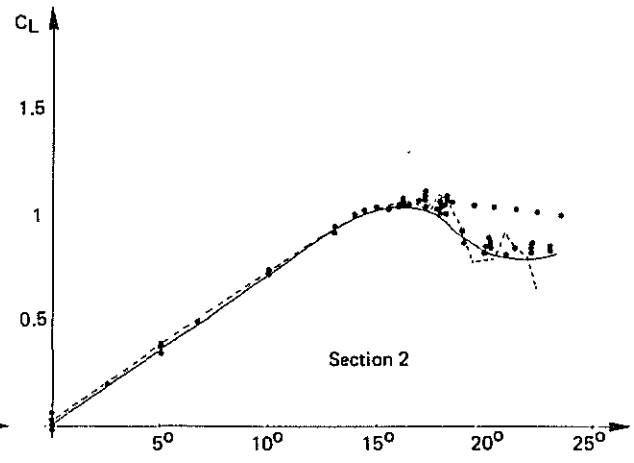

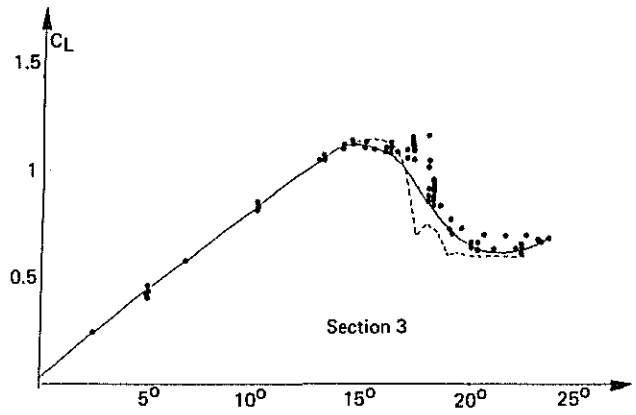

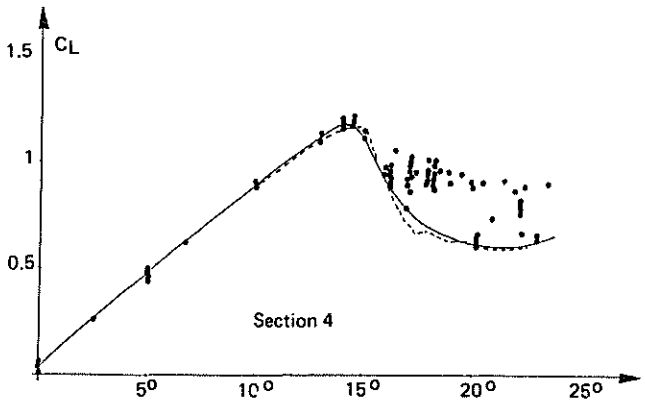

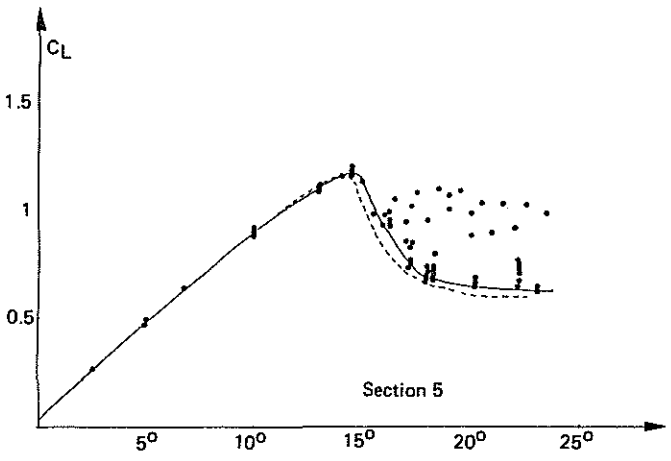

Fig. 6 — Lift distribution over the 5 instrumented sections: • Experimental data point ; — Experimental curve. Taken as the lower limit of the experimental points during stall ; ---- Theory.

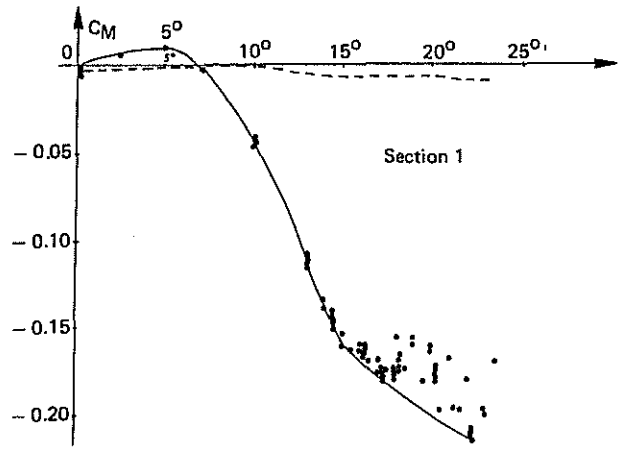

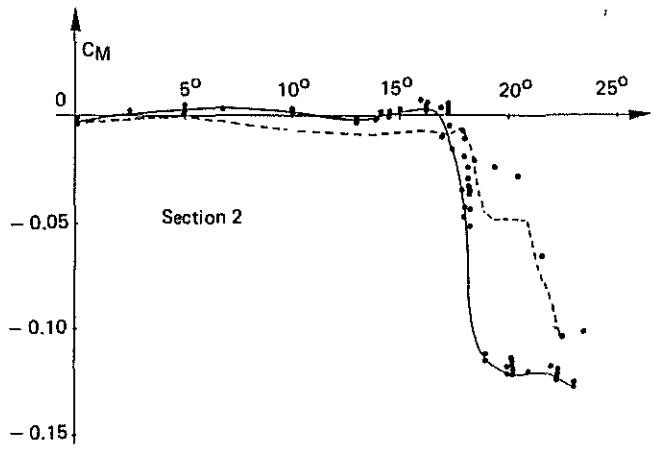

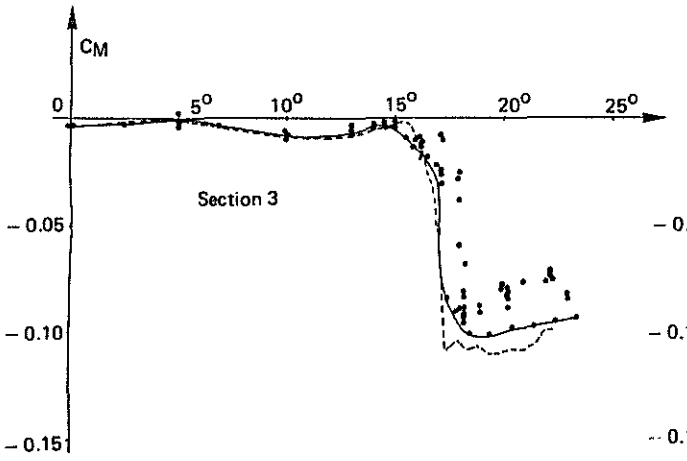

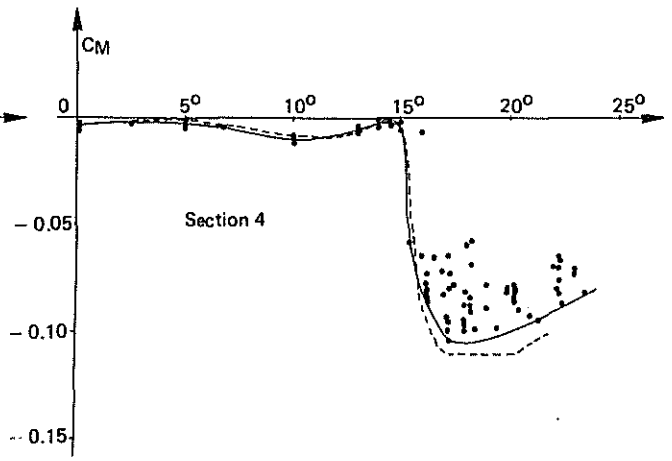

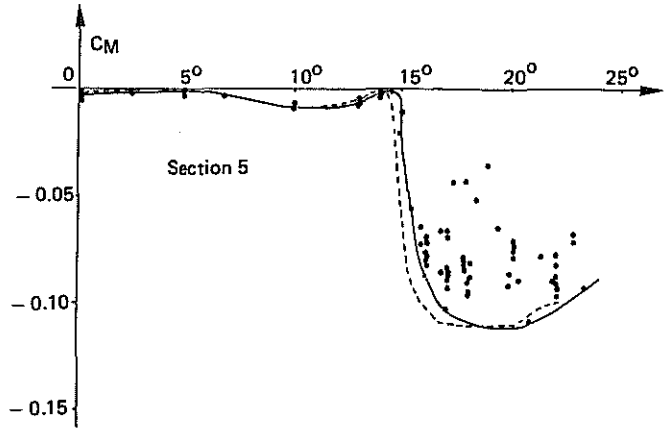

Fig. 7 — Moment around the quarter-chord measured and calculated for the 5 instrumented sections : • Experimental data points ; — Experimental curve. Taken as the lower limit of the experimental points during stall ; ---- Theory.

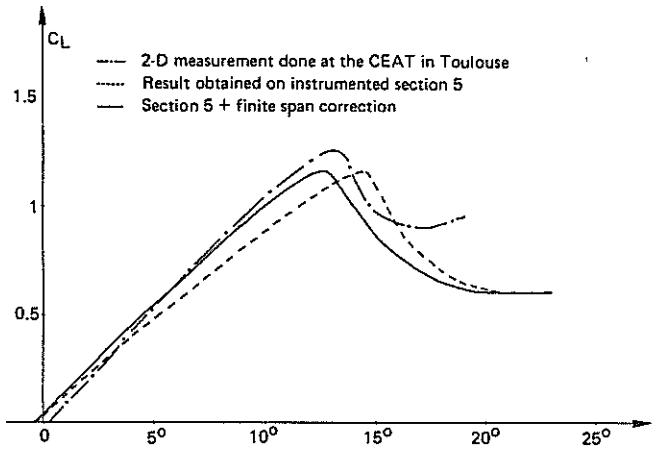

Fig. 8 — 2-D lift coefficient for the OA209 profile. Section 5 data + a finite span correction (solid line curve) is used in the 3-D theory : —·— 2-D measurement done at the CEAT in Toulouse ; ----- Result obtained on instrumented section 5; — Section 5 + finite span correction.

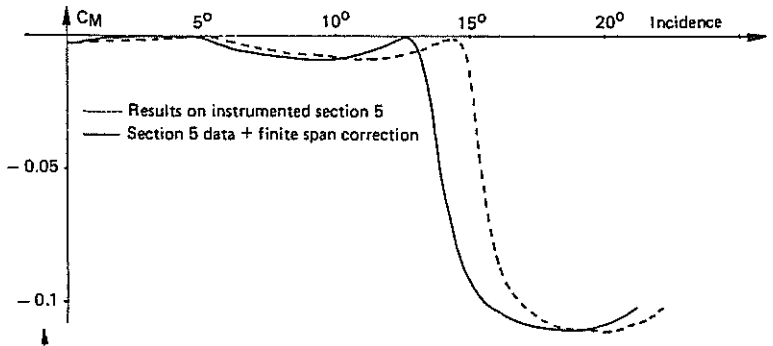

Fig. 9 — Moment coefficient around the quarter-chord for the OA209 profile. The solid line curve is used in the 3-D calculations : ---- Results on instrumented section 5 ; — Section 5 data + finite span correction.

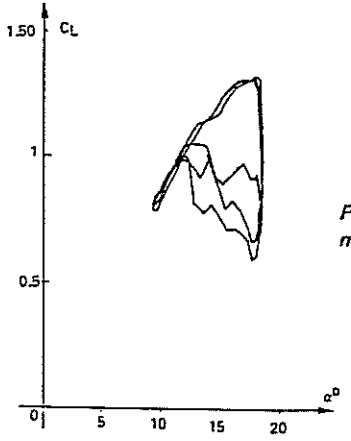

Fig. 10 — Time history of the lift coefficient for 3 successive cycles of oscillation measured on section 5. Incidence $14^o \pm 5^o$. Frequency 4.69 Hz - S2 Ch 1985.

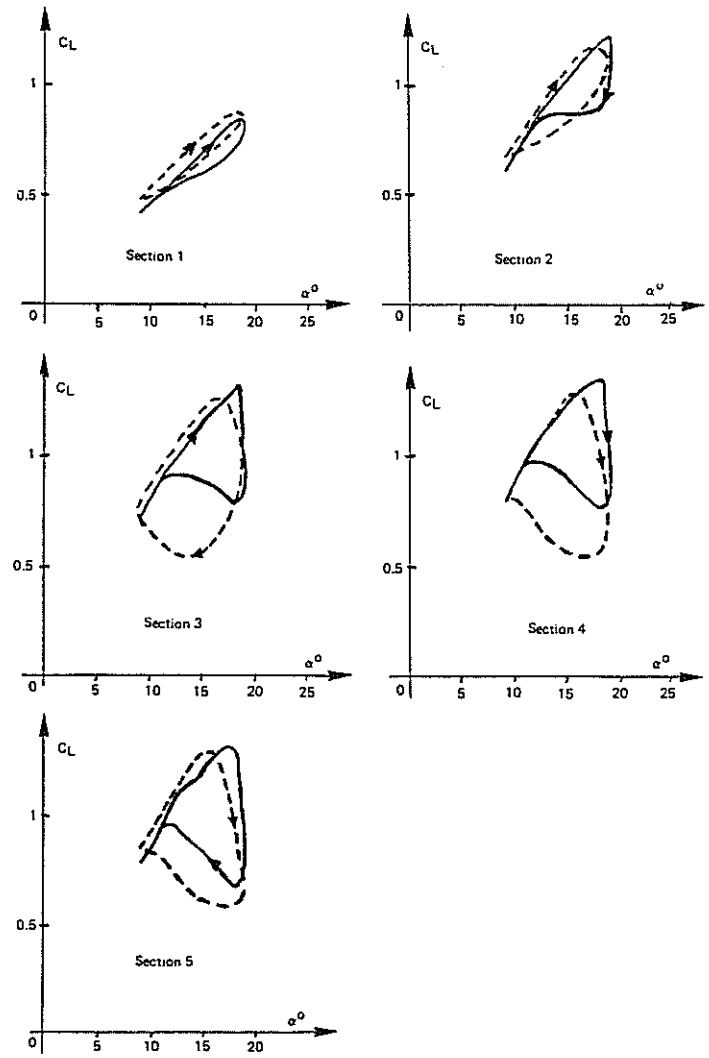

Fig. 11 — Incidence $\alpha^o = 14^o \pm 5^o$, Frequency 4.69 Hz Re = 1.72 10^6 ; — Exp. S2Ch 1985. ---- Theory. Standard 2D aerodynamic model for the OA 209 profile.

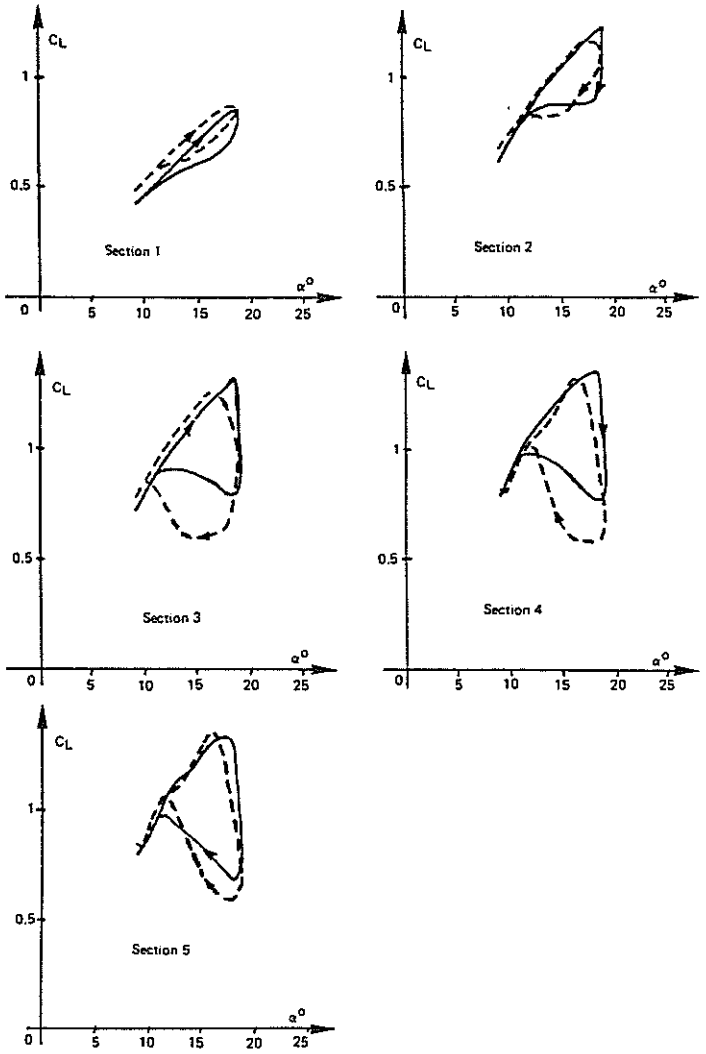

Fig. 12 – Incidence $\alpha^o = 14^o \pm 5^o$. Frequency 4.69 Hz Re = 1.72 10^6 ; — Exp. S2Ch 1985. ----- Theory. Modified 2D aerodynamic model for the OA 209 profile.

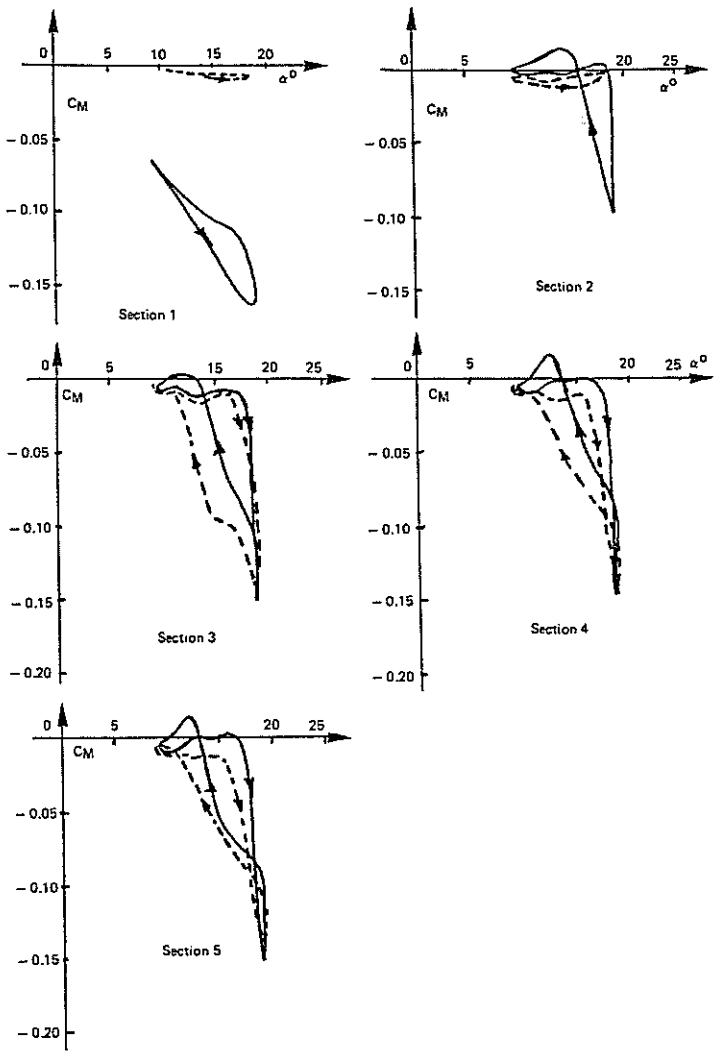

Fig. 13 – Incidence $\alpha^o = 14^o \pm 5^o$. Frequency 4.69 Hz Re = 1.72 10^6 ; — Exp. moments coeff. S2Ch 1985. ----- Theory.

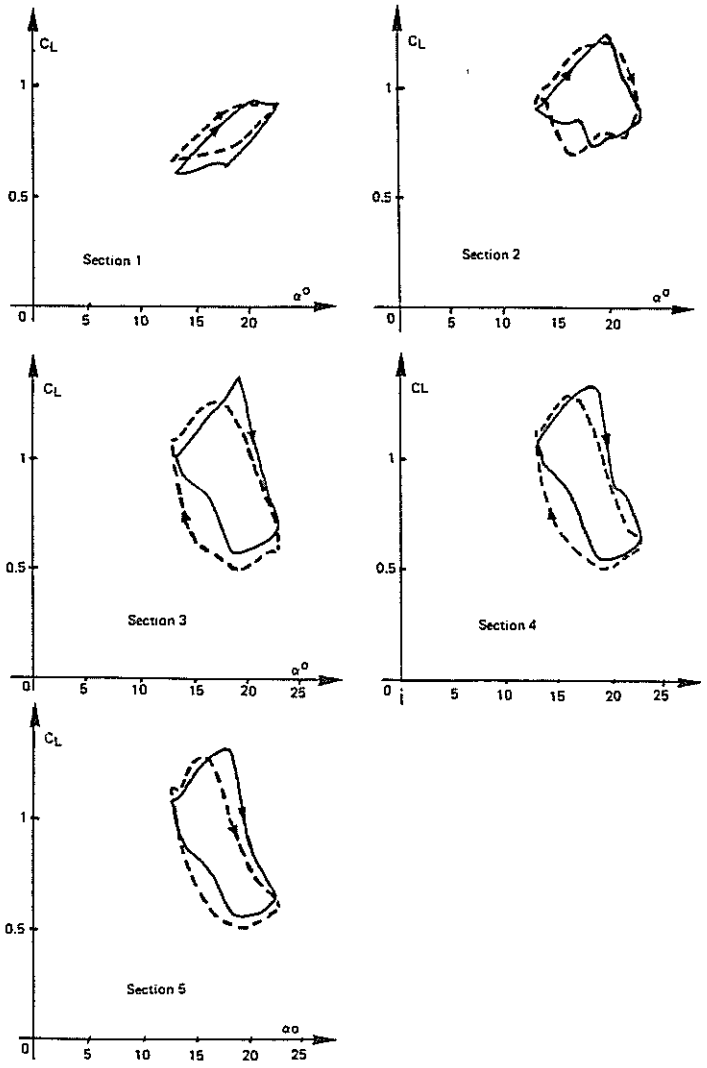

Fig. 14 – Incidence $\alpha^o = 18^o \pm 5^o$. Frequency 4.69 Hz Re = 1.72 10^6 ; — Exp. lift coeff. S2Ch 1985. ----- Theory. Modified 2D aerodynamic model for the OA209 profile.

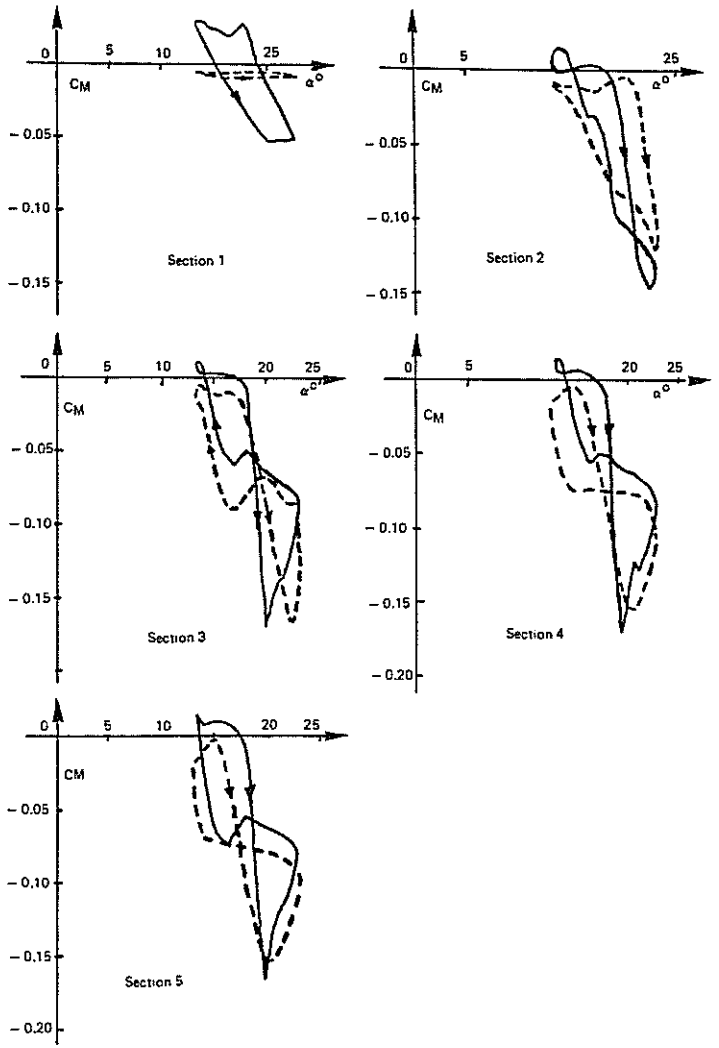

Fig. 15 – Incidence $\alpha^o = 18^o \pm 5^o$. Frequency 4.69 Hz Re = 1.72 10^6 ; — Exp. moment coeff. S2Ch 1985. ----- Theory.